The International Journal of Advanced Manufacturing Technology (2018) 97:3371–3384
https://doi.org/10.1007/s00170-018-2131-6

ORIGINAL ARTICLE

A low-density pulse-current-assisted age forming process for high-strength aluminum alloy components

Y. Q. Xu [1,3] · C. Y. Tong [1] · Lihua Zhan [1,2,3] · C. H. Liu [2,3] · J. S. Tan [2,3] · M. H. Huang [1,2,3] · Y. L. Yang [2] · H. Li [1,3]

Received: 14 December 2017 / Accepted: 6 May 2018 / Published online: 25 May 2018

Abstract

A pulse-current-assisted age forming process of the Al alloy component is developed and evaluated by simulation and experiments. The effect of pulse-current on the electric current density distribution, Joule heat effect, springback, mechanical properties, and precipitation microstructure of a 2219 Al alloy plate component is investigated. The results show that the current distribution is centrosymmetric in the component and the Joule heat effect under the low-density pulse current (less than 80 A/cm^2) can be ignored. Compared with the traditional age forming process, the pulse-current-assisted age forming process can reduce the springback and the shape deviation. This should be related to the pulse-current promotion of dislocation movement. At the same time, it restrains the coarse θ′ phase precipitation and homogenizes the precipitate distribution. Therefore, both the mechanical properties and electrical conductivity are increased evidently. Therefore, the pulse-current-assisted age forming process can improve the forming efficiency and precipitate microstructures, as well as the comprehensive performance, making it a potential cooperative manufacturing technique for better control of the shape and performance of high-strength aluminum alloy components.

Keywords Age forming · Pulse-current · High-strength aluminum alloy · Springback · Mechanical properties · Electrical conductivity · Precipitate microstructures

1 Introduction

High-strength aluminum component plays an important role in modern aerospace industry [1–4], supporting the requirements of structural weight reduction and performance improvement. Age forming technology, a combination of forming and aging, is an advance technique for the manufacture of high-strength aluminum components [5–7]. However, it is very difficult to improve the forming efficiency and performance of these aluminum components by regulating the process parameters (i.e., the temperature is limited to the age temperature and the applied stress cannot exceed the yield stress of the aluminum alloy). Therefore, it is necessary to develop an optimized age forming process for the high-strength aluminum components.

In the past, many meaningful experiments had been made to improve the age forming process [4, 8–15]. On the one hand, researchers added pre-treatment to obtain a desire initial temper of components and then achieved the target requirements. Xu et al. [8] experimentally investigated the pre-strain on constant-stress creep aging behavior of 2524 aluminum alloy. Yang et al. [9] studied the effect of the pre-strain on the springback, microstructures, and mechanical properties of age-forming component of AA2219 and found that pre-strain can effectively reduce the springback, improve microstructure, enhance the mechanical properties, and decrease the anisotropy inside the component surface. Zhang et al. [10] investigated the influence of pre-bending on the age-forming plate of AA7475 and concluded that pre-bending can improve the limit of the age forming. Li et al. [11] presented solid solution performed in electric field before age forming, which displayed better formability and elongation than traditional solid solution. It is worth noting that the presence of extensive

✉ Lihua Zhan
yjs-cast@csu.edu.cn

[1] Light Alloy Research Institute of Central South University, Changsha 410083, People's Republic of China

[2] College of Mechanical and Electrical Engineering of Central South University, Changsha 410083, People's Republic of China

[3] State Key Laboratory of High-Performance Complex Manufacturing, Central South University, Changsha 410083, China

range of alloy elements in aluminum matrix made it susceptible to precipitate evolutions, which may have strong influence on the arising defects such as springback effect [4]. Therefore, new alloys of the 2XXX series are being developed for CAF application [12–14]. Some of them belong to the latest generation of Al–Cu–Li alloys, such as AA2050. In addition, the 5XXX Al–Mg series alloys containing scandium have been developed for creep forming [15]. Those alloys, such as AA5024, are not precipitation hardenable, and this is why their process was named creep forming (CF) instead of CAF. Although the strength of such alloys is weaker when compared to 2XXX and 7XXX series alloys, higher creep rates can be achieved in such alloys, as the scandium content promotes microstructural stability enabling the CF to be processed at significant higher temperatures (above 400 °C). Corrosion, fatigue, and fatigue crack growth performance of such alloys are also quite interesting, especially for fuselage skin applications.

On the other hand, by means of multistep heat treatments and additional energy field during the age forming process, the forming efficiency and comprehensive performance of the component were improved. Jeshvaghani et al. [16] explored the impact of multistep heat treatments on the springback, strength, and corrosion resistance in CAF and found that multistep heat treatments are able to lessen the springback and heighten the corrosion resistance while maintaining the strength. Huang et al. [17] applied electric field in the age forming process of AA7075, which promoted stress relaxation and formability. The higher the electric field intensity is, the better the results are. Zhan et al. [18] investigated the effect of alternating electrical pulse with different frequencies on the structure and performance of AA7075 and suggested a significant improvement on structure and properties of aluminum alloys under aging companying with alternating electrical pulse. Also, Zhan et al. [19] introduced an electric pulsed current into the stress relaxation aging process of 2219 aluminum. They found that the electric pulsed current can effectively regulate the stress relaxation behavior during the initial aging stage. That is, the application of electric pulsed current during the first 1 h of the aging treatment process decreases the stress gradients for different initial stress levels, which makes it possible to reduce the deformation and phase transformation inhomogeneities resulting from stress differences inside a component under a bending load. Meanwhile, the apparent deformation activation energy decreases with the electric pulsed current, by which the energy barrier difference between the stress relaxation and aging precipitation is decreased from 47 to 18 kJ/mol. Therefore, pulse current may be introduced into the age forming process to achieve high-performance and high-precision collaborative manufacturing of large aluminum alloy component. In view of above, almost studies on pulse-current-assisted age forming process are conducted at the sample scale, in which the pulse current is uniform and the applied stress is simple. In fact, the current field and the stress state vary from place to place in component during the pulse-current-assisted age forming process. Thus, it is necessary to investigate the role of the pulse-current in the age forming process of aluminum alloy components.

In this work, the pulse-current-assisted age forming process and its equipment are introduced. Then, the current distribution and its Joule heat effect are investigated. The Joule effect and current density distribution of the component during the pulse current assisted age forming process are simulated by Comsol Multiphysics software. The pulse-current-assisted age forming tests of 2219 aluminum alloy components are conducted and the traditional age forming tests are referenced. The springback of these two processes formed component is evaluated. In addition, mechanical property tests and transmission electron microscopy (TEM) observation are carried out. The research will develop and evaluate the pulse-current-assisted age forming process for high-strength aluminum alloy component manufacture.

2 Material and experiment

2.1 Material

The received material is the 2219 aluminum alloy hot rolling plate supplied by Southwest Aluminum Company. Four components with the size of 420 mm × 250 mm × 8.5 mm are cut out along the rolling direction of the sheet by the hydraulic shearing machine. According to the heat treatment of 2219 aluminum alloy [20], solution and quenching are applied to the plates before age forming process. The solution temperature is 535 °C and the plates will be hold at this temperature for 1 h. The plates are water (room temperature) quenched within 35 s after solution treatment. In order to protect the vacuum bag and the insulating film during the age forming tests, the components are polished using waterproof abrasive papers (Table 1).

2.2 Pulse-current-assisted age forming tests

The pulse-current-assisted age forming test is carried out on an autoclave (YT-14-03, China) equipped with an electric pulse power, as shown in Fig. 1. The pressure control accuracy is ± 0.005 MPa and the temperature field uniformity is ± 2 K. The electric pulse power (Fig. 1a) is a self-developed high-power device (three-phase alternating current input power 380 V/50 Hz/50 kVA, positive pulse, adjustable pulse current 0–5400 A; current frequency 100~1000 Hz; adjustable duty cycle 10–90%). In addition, the cooper wires and soft conductors are also included for the connection between the electrical pulse power and the component in autoclave, as shown in Fig. 1b, c. It is noteworthy that the soft conductors with a

Table 1 The main chemical composition of 2219 aluminum alloy (mass percentage, %)

Chemical composition	Cu	Mn	Si	Fe	Mg	Zn	Zr	Al
Mass fraction	5.8–6.8	0.2–0.4	0.2	0.3	0.02	0.1	0.1–0.25	Bal.

radius of 60 mm are used to adjust the best contact between the deformed plate and mold. In addition, five thermocouples are applied to record the temperature during the forming tests.

In this work, both the pulse-current-assisted and traditional age forming tests are carried out. The mold with the radius of 1167 mm is used. The pulse-current-assisted age forming process procedures is shown in Fig. 2. Before age forming tests, the 2219 aluminum plates were solution treated at 808.15 K for 0.5 h. Similar to the traditional age forming process (Fig. 2a) [8, 21], the electric pulse assisted age forming process mainly include three steps that are (1) loading, (2) electrical pulse assisted age forming, and (3) unloading. The details of the electrical pulse assisted age forming process are shown in Fig. 2b. In the loading process, the vacuum pressure of 0.1 MPa was applied outside the autoclave for assembling the plate and tools (the mold, ventilated felt, vacuum bag, and thermocouples). Then, the assembly was submitted to the autoclave and the autoclave pressure was raised to the working pressure of 0.5 MPa to force the plate completely molded the mold surface. In the forming process, the aging temperature is 438.15 K and hold for 8 h. The heating rate of 2 K/min and naturally cooling in autoclave is used, respectively. Based on the previous works [22–24], a set of lower electric pulse parameters are optimized and recommended for creep aging of AA2219, which is positive pulse current, average current density of 80 A/cm^2, duty cycle of 50%, and frequency of 500 Hz. The electric pulse is applied within the first 1 h when the temperature is stable at the aging temperature. The traditional age forming test is consistent with the electrical pulse assisted age forming test, except that the electrical pulse is not applied during the forming process. When the forming process is finished, the autoclave pressure and vacuum pressure are unloaded in order. Due to the limitations on the maximum usable temperature and the forming time dictated by microstructure requirements, the workpiece definitely springs back after unloading.

2.3 Springback test

The magnitude of plate's springback [8, 25] is quantitatively represented by the following:

$$SP = (1-R_0/R_f) \times 100\% \quad (1)$$

Where SP denotes the amount of springback, and the smaller the SP value is, the more accurate the configuration of deformed plate is; R_0 and R_f refer to the bending radius of the plate before and after unloading process. The Atos Raster Scanner (GOM, Germany) scans the surface (the one in contact with tool surface) of the formed component. The accuracy

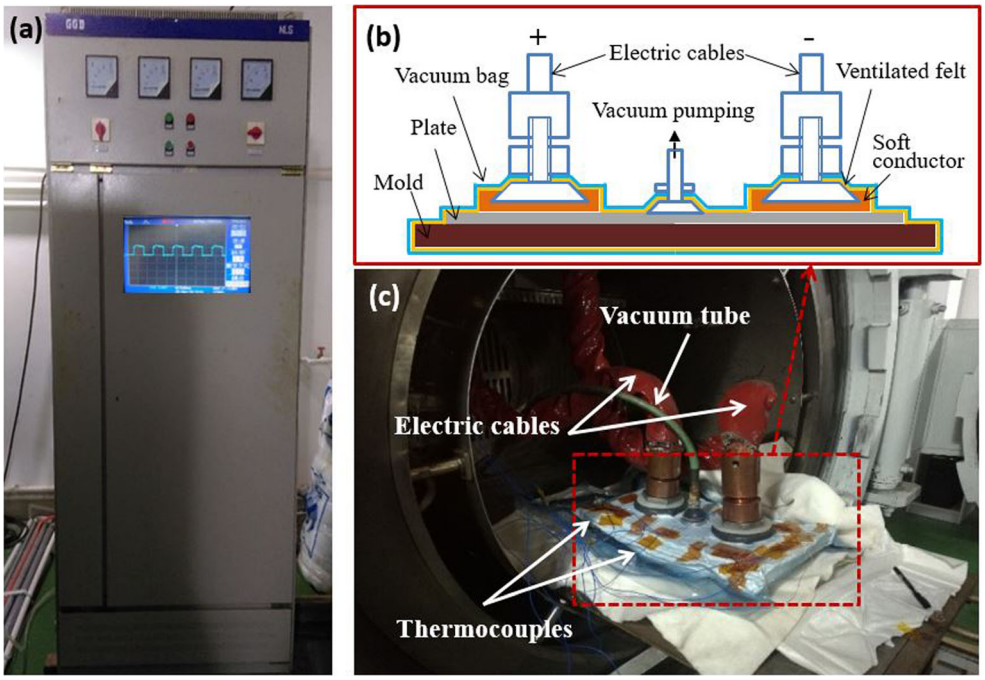

Fig. 1 Schematic diagram of pulse-current-assisted age forming in an autoclave. **a** Electric pulse power. **b** Assembly schematic diagram. **c** Assembled objects

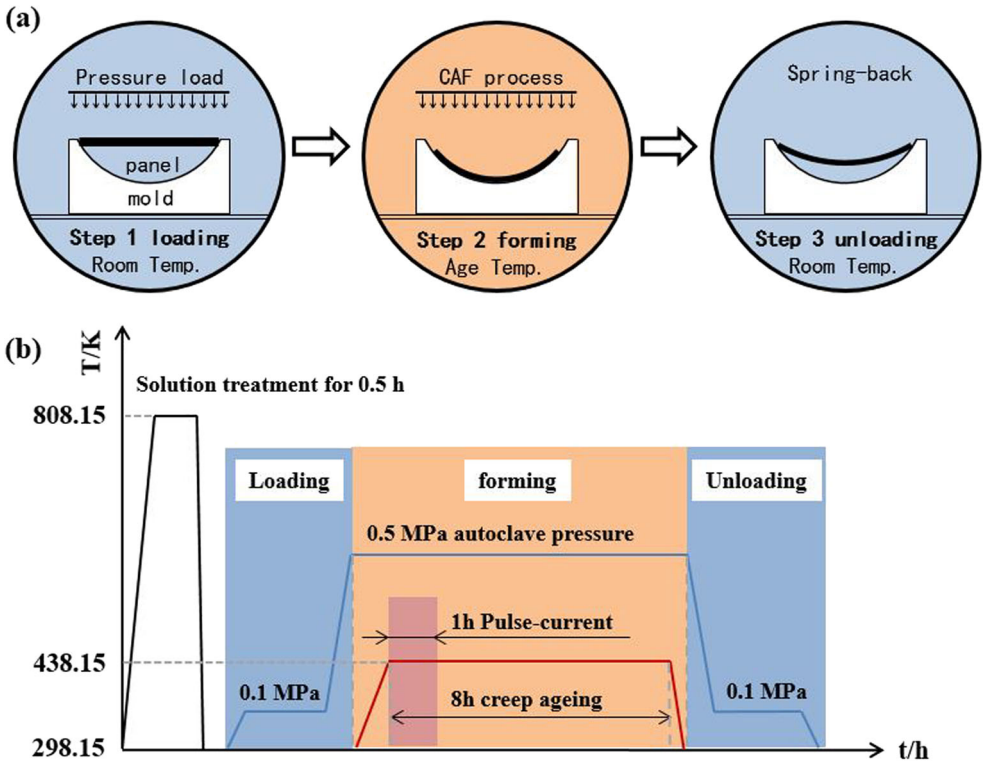

Fig. 2 The pulse-current-assisted age forming process procedures

of this Atos Raster Scanner is 0.01 mm per meter. Since the springback of each part of the formed component is not exactly the same, the surface is divided into five parts along the width direction, and the average value is taken as the curvature radius of the component.

2.4 Mechanical property test

The mechanical property test is carried out on the CMT-5504 electronic universal testing machine at room temperature. In order to investigate the effect of electric pulse on mechanical property anisotropy of the formed component, the tensile samples are cut from the component at 0°, 45°, and 90° angles to the rolling direction. Moreover, the component is subjected to bending so that one side of the component is in tension and the other side is in compression. Therefore, the investigation of the mechanical property difference between the lower surface (under the tensile stress) and upper surface (under the compressive stress) of component also is carried out. The tensile samples are manufactured according to national standard [16] metal sheet tensile specimen size with the gauge length of 30 mm. Two samples were taken in each direction and the average of the two results was applied. The anisotropy index of the mechanical properties is calculated by following equation:

$$IPA = \frac{2X_{\max} - X_{mid} - X_{\min}}{2X_{\max}} \times 100\% \quad (2)$$

where $X_{\max}$, X_{mid}, and $X_{\min}$ denote the maximum, intermediate, and minimum values of the mechanical properties in the three directions of the component, respectively.

2.5 Electrical conductivity tests

The electrical conductivity tests are carried out on the SIMASCOPE SMP350 measuring instrument. The formed plates were grinded to remove the oxide film from the surface with 800 # water sand paper. A hand-held probe of 10 mm diameter was utilized to measure the conductivity in units of %IACS (International Annealed Copper Standard). A series of electrical conductivity are measured at 30 equispaced points on both sides (upper and lower surfaces) of the tradition age formed and pulse-current-assisted age formed components, as well as the solution treated one.

2.6 Microstructure observations

The precipitate microstructure of the formed components is observed by JEM-2100F field emission high-resolution transmission electron microscope (TEM). The transmission sample was first processed into a φ3-mm disk and mechanical polished to 60 μm thin and then sprayed by the mixed liquor of 30%HNO3 + 70%CH3OH. The voltage is 15 V and the temperature is − 30~− 20 °C.

3 Results and discussion

3.1 Joule effect and current density distribution during the pulse current assisted age forming process

In the pulse-current-assisted age forming process, the pulse-current is applied through two soft conductors binding on the component. The current density distribution is difficult to be quantitatively measured by experiments. In addition, the current will produce Joule effect causing temperature rise of the plate. Therefore, it is necessary to choose a suitable current density to avoid unwanted temperature changes in component during the pulse current assisted age forming process.

In order to investigate the current density and Joule effect, the AC/DC and the heat transfer modules in Comsol Multiphysics [23] are used as shown in Fig. 3. The geometric model is shown in Fig. 3a. The tetrahedral element is adopted to mesh the 3D geometric, and the regional mesh near the conductive plate is localized, as shown in Fig. 3b. Assuming that the pulse current is transmitted from one of the soft conductor to another through the component. During the pulse-current-assisted age forming process, the temperature of the component is 438.15 K. The air temperature in autoclave is 438.15 K (ambient temperature of age forming process) and the heat transfer coefficient is 5 W/(m^2▪K). In addition, the material properties of 2219 aluminum alloy and cooper are shown in Table 2.

The creep aging process of aluminum alloy is sensitive to temperature [26, 27]. Current density will cause an increase in temperature of aluminum alloys. The higher the current density is, the greater the Joule heat effect of the material is. Therefore, appropriate current density parameters must be considered to avoid the Joule heat effect. Figure 4 shows the relationship between the current density and temperature rise after 1-h pulse current assisted creep age forming process. It can be found that the temperature rise increases with the

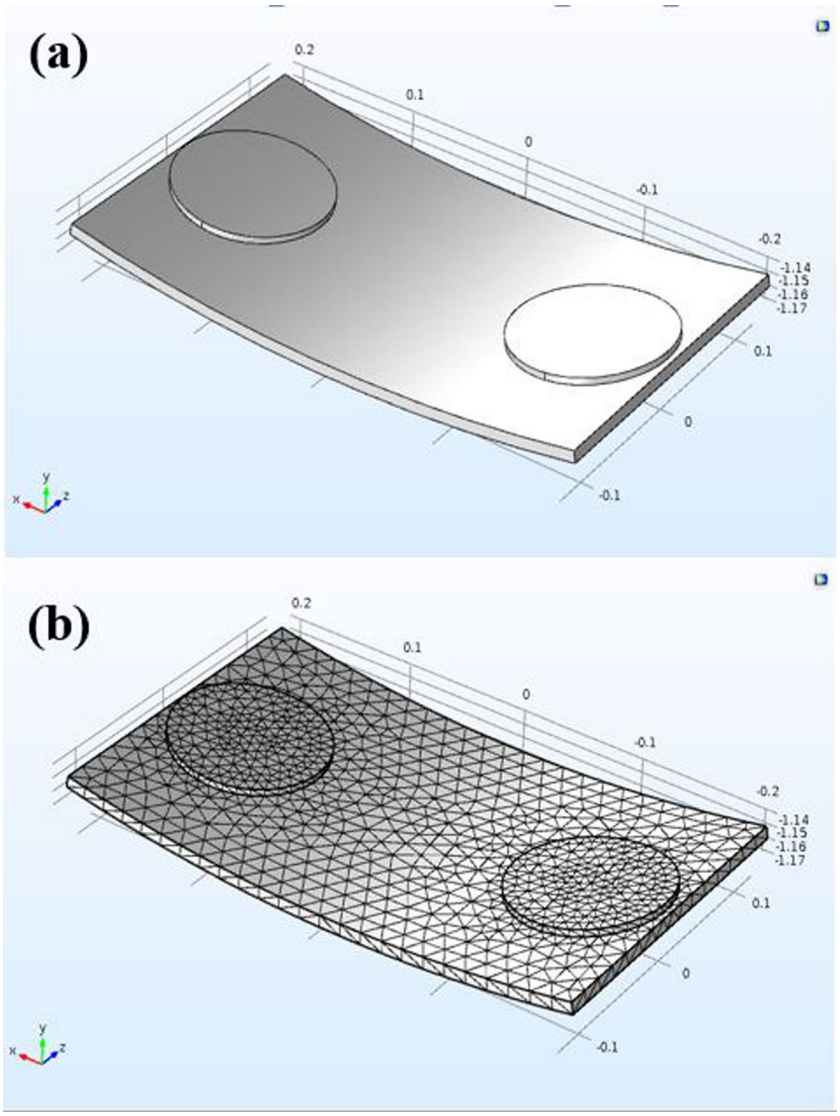

Fig. 3 Component geometry model (**a**) and meshing (**b**)

Table 2 Material properties of 2219 aluminum alloy component and conductive plate

Materials	Properties	Parameters
Conductive plate (copper)	Conductivity	5.998e7 S/m
	Atmospheric heat capacity	385 J/(kg K)
	Relative permittivity	1
	Density	8960 kg/m^3
	Thermal conductivity	400 W/(m K)
Aluminum alloy component (AA2219)	Conductivity	3.744e7 S/m
	Atmospheric heat capacity	900 J/(kg K)
	Relative permittivity	1
	Density	2700 kg/m^3
	Thermal conductivity	238 W/(m K)

increase of the applied current density. When the peak current density of the pulse current is 80 A/cm^2, the temperature rise of the alloy is about 0.95 K. When the current density increases to 220 A/cm^2, the temperature rise caused by the current exceeds 5 K. Therefore, the low-density pulse current of 80 A/cm^2 is chosen to carry out further research.

Figure 5 shows the current density field of the component during the age forming process with the peak current of 80 A/cm^2. It can be seen from Fig. 5 that the current density in the center of the component is relatively higher than that in the area around the component. However, the edge of the conductive plates that contacts the component has the greatest current density of 86.7 A/cm^2 and the component's corners have the lowest current density of 4.38×10^{-3} A/cm^2. The current density of the area between the two soft conductors is 25~45 A/cm^2.

Figure 6 indicates the temperature distribution of the component after 1-h electric pulse assisted age forming process. It is expected that the distribution of temperature field is similar to that of current density field. However, the temperature difference of the component after 1-h electric pulse assisted age forming process is not significant. In Fig. 6, the maximum temperature of the component is 439.1 K, and the temperature rise is less than 1 K (438.15 K as reference).

In addition, five thermocouples are attached to the center of the upper surface of the component to record the temperature changes during the age forming processes. The temperature difference between the area with and without pulse-current assisted is less than 1 K, which is consistent with the simulation result with the current density of 80 A/cm^2. The results of comprehensive simulation and experimental results show that the low-density pulse current will not produce significant change in component's temperature and the Joule effect on the aging temperature can be ignored under the test condition.

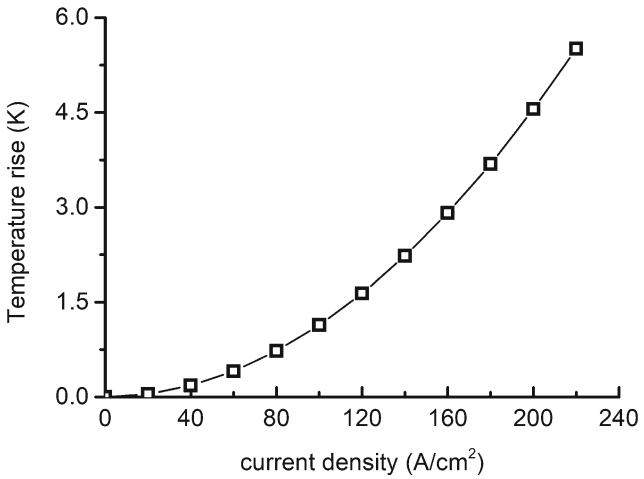

Fig. 4 The relationship between the current density and temperature rise after 1-h pulse current assisted creep age forming process

3.2 Effect of electrical pulse on springback of the formed components

In general, springback does not occur uniformly in the plate, so the radius of 5 sections of formed plate along the width direction (Fig. 7a) were measured, respectively, with radius distribution shown in Fig. 7b. It is found that both the age formed component and the electric pulse assisted age formed component, the radius of the section 3 is the largest one of the five radiuses. Meanwhile, the radii of sections 1 and 5 are smaller than other sections. Yang et al. [8] described that this result can be related to the fact that the ventilated felt will get caught between the gaps of the mold and plate in the process of vacuum-pumping, which increases the tool surface radii of two sides (section 1 and section 5) when compared to the middle area.

In Fig. 7b, the average radius of the traditional age formed component is 1687.8 mm and the springback is 30.86%. More positively, the average radius of the electric pulse assisted age formed component is 1536.1 mm and the springback is 24.03%. By comparison, the result shows that the springback of the electric pulse assisted age formed component is reduced by 22.13%. It is well-known that the springback of component is related to the creep deformation during age forming process. Creep deformation, during the age forming process, is mainly controlled by dislocation motion [28]. Under the condition of pulse current, the high-speed and high-energy electron flow hits the dislocations, which improves the movement of dislocations. Therefore, the component with electrical pulse is more prone to creep deformation, resulting in the lower springback of electrical pulse assisted age formed component. On the other hand, the standard deviation (STDEV for short) of the five radiuses for the formed components is also calculated (Fig. 7b). The standard deviation of the traditional age formed component and the electric pulse assisted age formed component is 15.87 and 11.20 mm, respectively. One possible reason is that, for an aluminum alloy component, the deformation of each region must be consistent with others. Namely,

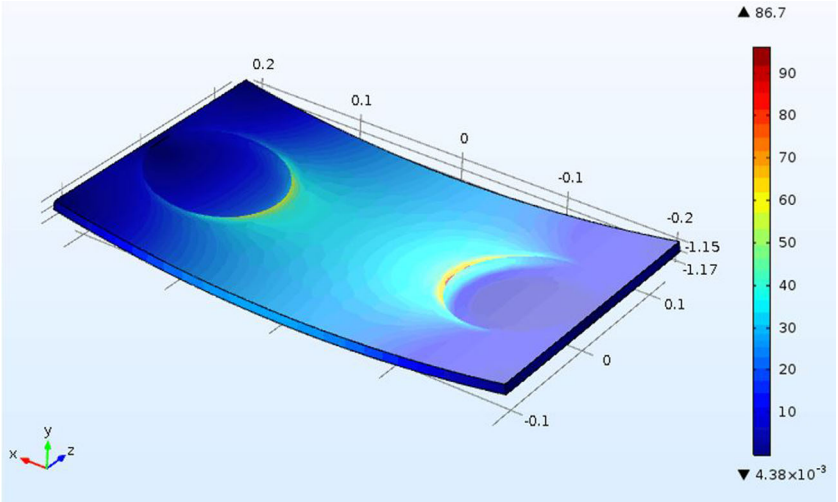

Fig. 5 The peak current density field of the component during the age forming process with the peak current of 80 A/cm^2

a slower deformation region blocks a region of faster deformation. It shows that the pulse current also improves the overall deformation coordination. Therefore, the low-density pulse current assisted age forming process can improve the forming efficiency and precision of the studied aluminum alloy component.

3.3 Effect of electrical pulse on mechanical properties of the formed components

The stress-strain curves of different samples in both the AFed and PCAAFed components are shown in Fig. 8. Figure 8a–c shows the stress-strain curves of the samples at 0°, 45°, and 90° three different orientations, respectively. Moreover, the yield stress-strain curves of both the compressive stress layer and tensile stress layer are carried out. The corresponding mechanical properties of the formed 2219 aluminum alloy components are reported in Table 3.

The pulse current has significant influence on the mechanical properties of the formed components. The flow stresses of the samples in PCAAFed component are greater than that in AFed component (Fig. 8). More details of the difference between the two forming process can be found from Table 3. In the PCAAF process and the AF process, the tensile/yield strength of the compressive stress layer is higher than that of the tensile layer of the formed 2219 aluminum alloy component. Meanwhile, the elongation of the compressive stress layer is significantly lower than that of the tensile stress layer. For example, comparing the mechanical properties in 0°orientation samples of PCAAFed component under tensile stress layers, the one under the compressive stress layers has 48.2 MPa higher in tensile strength, 20.25 MPa higher in yield strength, and 2.35% lower in elongation. It indicates that the performance of the formed component in the thickness direction is asymmetric and significantly affected by the stress state. On the other hand, the mechanical properties of the formed components in various orientations are different.

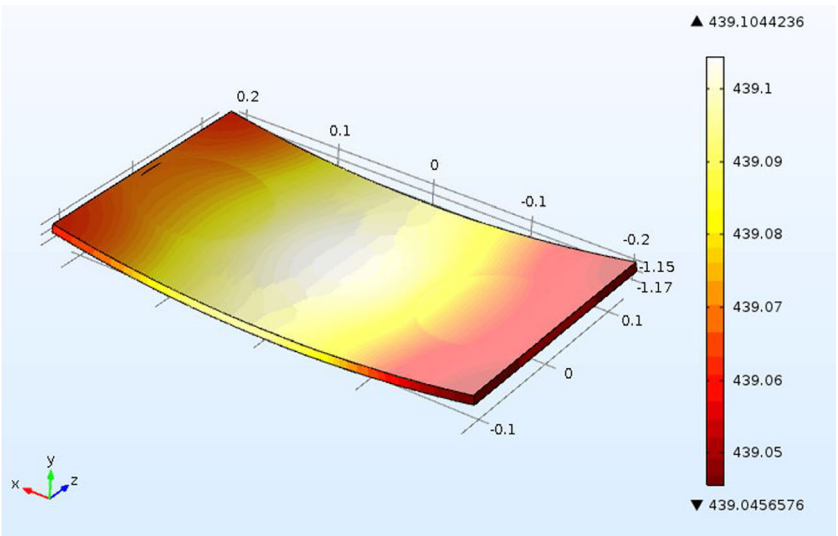

Fig. 6 Temperature distribution of the component after 1-h pulse current assisted age forming process

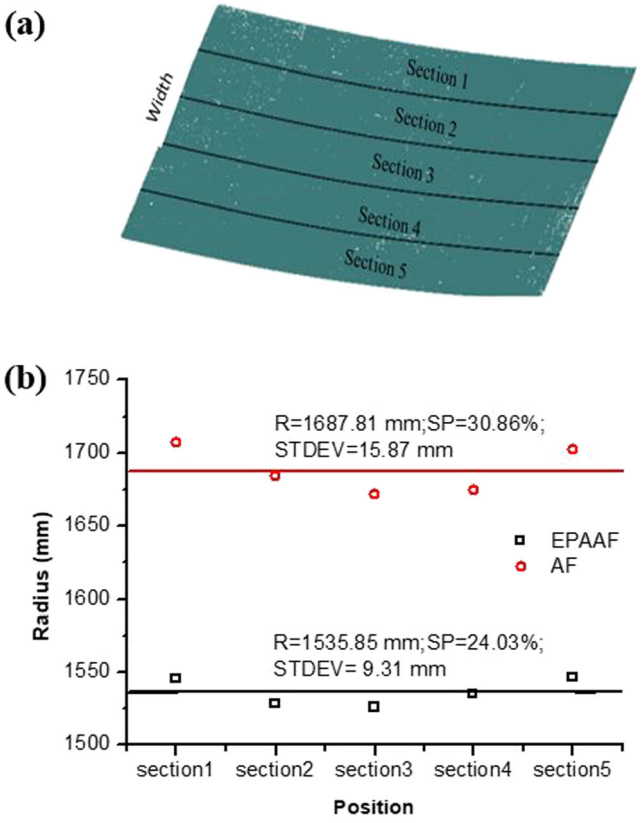

Fig. 7 Springback of the formed components. **a** Example of measuring the radius of the partition. **b** Radius of different areas

With the angles between the rolling direction and applied stresses increase, the tensile/yield strength increased and the elongation decreased. The IPA value describes the degree of the planar anisotropy. It is reported from Table 3 that the IPA values of the mechanical properties are less than 5% in both two forming processes. It suggested that the mechanical property anisotropy of the formed component is not obvious. In addition, there is no significant difference between the IPA value of the two forming process, indicating that the pulse current has no obvious effect on the mechanical property anisotropy of the studied component.

The pulse-current has a positive effect on mechanical properties as shown in Fig. 9. Figure 9a shows that the mechanical properties in 0° orientation samples of formed components within tensile stress layer. As shown in Fig. 9a, the tensile strength increases from 356 to 388 MPa, the yield strength improves from 245 to 252 MPa, and the elongation slightly decreases from 18.4 to 17.2% under the condition of pulse current. For the samples in compressive stress layers (Fig. 9b), the tensile strength and yield strength of the PCAAFed component have improved by 15 and 10 MPa, respectively. Interestingly, the elongation of the samples with and without electric pulse assisted is almost the same. It showed that the pulse current assisted age forming process could enhance the strength of the 2219 aluminum alloy component.

Based on the mechanical property difference (Table 3) between the compressive stress layer and the tensile stress layer, we can further analyze the effect of pulse current on the consistency of mechanical properties within age formed component. Figure 9c shows the comparison of the relative difference percentage (RDP) of the tensile strength, yield strength, and elongation in the 0° orientation samples of the age formed and the pulse-current-assisted age formed components. It can be found that the RDP of the tensile strength and elongation in the PCAAFed component are significantly lower than that in AFed component (Fig. 9c). The RDP in the tensile strength, yield strength, and the elongation of the 0° orientation samples within the AFed component is 15.4, 7.1, and 20.7%, respectively. For the 0° orientation samples within the PCAAFed component, the RDP is 11.1, 7.4, and 13.7% in order. Despite of the yield strength difference in the PCAAFed component is slightly higher than that in the AFed component, the positive effect of the pulse current on the mechanical properties is observed. It indicated that the low-density pulse current assisted age forming process could improve the consistency of mechanical properties within the studied aluminum alloy component.

3.4 Effect of electrical pulse on electrical conductivity of the formed components

The electrical conductivity of the alloy depends on the electrons' mobility in crystalline structure of material. In other words, all the strengthening mechanisms lead to additional distortions in the lattice structure and provide an additional increase in the electrical resistivity of metallic materials. The Matthiessen's rule for calculation of additional resistivity is as follows [29, 30]:

$$\rho_{total} = \rho + \rho_{ss} + \rho_p + \rho_d + \rho_{gb}$$

where ρ total is the total resistance, ρ is the electrical resistivity of the lattice, ρ_{ss} is the resistivity which comes from solute atoms dissolved within matrix, ρ_p is the resistivity of second-phase precipitates, ρ_d is the presented resistivity by the microstructure dislocations, and ρ_{gb} is the resistivity associated with grain boundaries. Meanwhile, ρ_p would be related to other types of precipitates (i.e., GP zones. incoherent and coherent precipitates). Among them, the ρ_{ss} and ρ_p (for GP zones) have the greater portions in ρ_{total}.

Figure 10 shows the electrical conductivity of the solution treated, age formed, and pulse-current-assisted age formed 2219 aluminum alloy plate. It can be found that, in solution state, the average electrical conductivities of both sides are 30.3 %IACS. During the age forming process, the change of dislocation and grain boundary is little due to the condition of low temperature and applied stress. Therefore, the electrical conductivities change after the two different forming

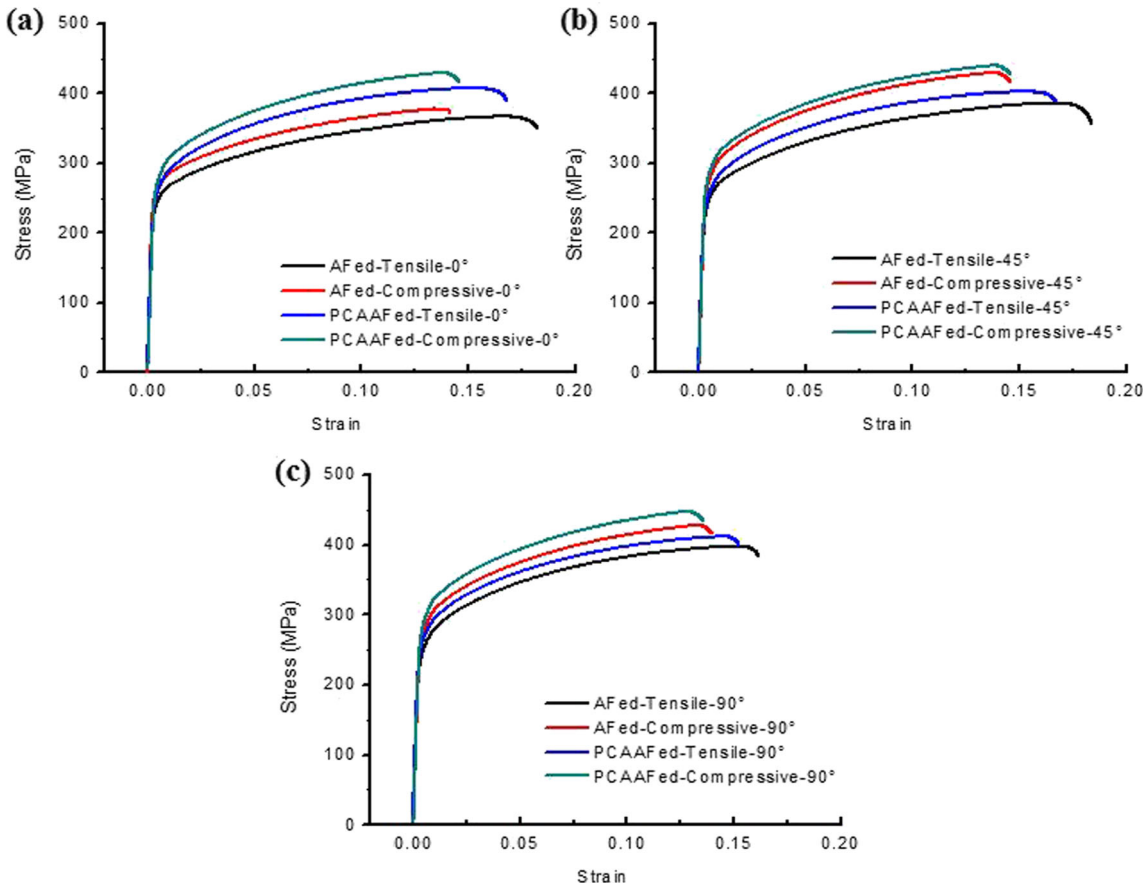

Fig. 8 The stress-strain curves of different samples in both the AFed and PCAAFed components at **a** 0° orientation and **b** 45° orientation and **c** 90° orientation

processes mainly caused by the degree of solid solution and precipitation. During aging process, the supersaturated solid solution obtained by quenching will gradually precipitate, which reduces the degree of lattice distortion of the alloy. Therefore, the electrical conductivity of both AFed and PCAAFed components are significantly higher than that of the solution-treated plate. For the age formed component, the increments of electrical conductivity in compressive stress layer and tensile stress layer are different. The electrical conductivity in the tensile stress layer is significantly higher than that in compressive stress layer. Similar results are found in the pulse-current-assisted age formed component. However, compared with the electrical conductivity of the age formed component, the electrical conductivity response in both sides of the pulse-current-assisted age formed component is greater. This means that the stress crack corrosion resistance in the pulse-current-assisted age formed component is better than that in the traditional age formed component.

Table 3 Mechanical properties of the formed 2219 aluminum alloy components

Forming processes	Orientation	Tensile stress layer/compressive stress layer (difference)		
		Tensile strength (MPa)	Yield strength (MPa)	Elongation (%)
AF	0°	356.31/421.05(64.74)	245.23/263.78(18.55)	18.4/14.56(3.84)
	45°	373.06/430.99(57.93)	248.81/266.66(17.85)	18.95/14.26(4.69)
	90°	380.47/435.30(54.83)	255.42/269.28(13.86)	18.34/13.51(4.83)
	IPA(%)	4.1/2.1(2.0)	3.3/1.5(1.7)	3.1/4.6(1.5)
EPAAF	0°	388.29/436.49(48.2)	252.86/273.11(20.25)	17.20/14.85(2.35)
	45°	395.97/440.73(44.76)	260.04/281.06(21.02)	17.34/14.89(2.45)
	90°	404.82/448.89(44.07)	266.61/283.33(16.72)	16.66/13.97(2.69)
	IPA(%)	3.1/2.3(0.8)	3.8/2.2(1.6)	2.4/4.9(2.5)

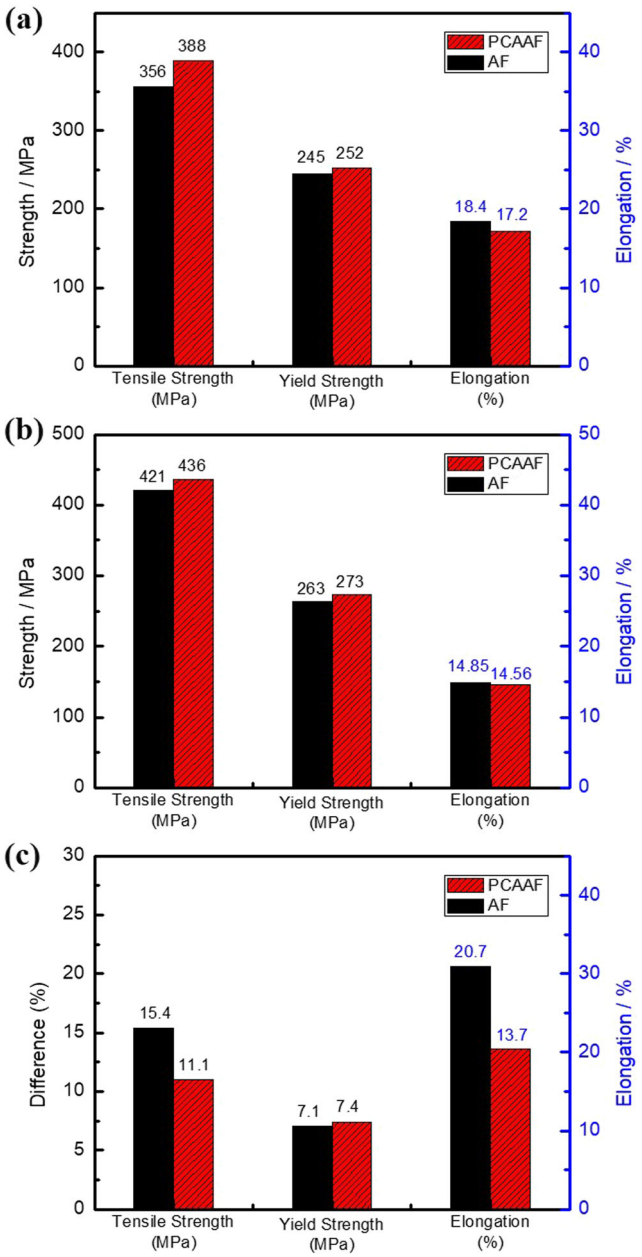

Fig. 9 Comparison of the mechanical properties between the PCAAFed and AFed component within **a** tensile layers, **b** compressive layers, and **c** their differences

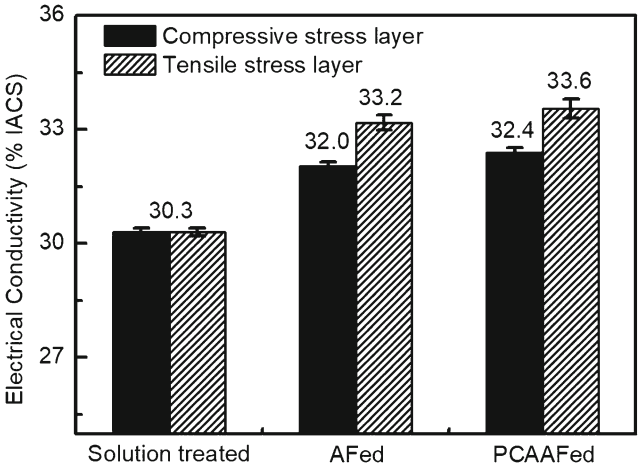

Fig. 10 Comparison of the electrical conductivity between the PCAAFed and the AFed component within **a** tensile layers and **b** compressive layers

3.5 Effect of electrical pulse on microstructure of the formed components

Microstructures determine mechanical and physical properties of materials. In order to investigate the effect of pulse current on the microstructures of the two types age formed component, the precipitate microstructures of the tensile stress, and compressive stress layers in the studied component after the traditional age forming process (Fig. 11) and the pulse current assisted age forming process (Fig. 12) are observed, respectively. Generally, the precipitate sequence of Al-Cu alloys has been proposed: SSS → GP zones→θ″ → θ′ → θ [31], where SSS stands for supersaturated solid solution and GP zones represents the Guinier-Preston zones. GP zones and θ″ are coherent second phase. θ′ and θ are the semi-coherent and equilibrium phase. Moreover, the misfit between θ sequence and Al matrix can be determined based on the orientation relationship of $\{100\}_{\theta}//\{100\}_{Al}$.

Figure 11 is the TEM images and corresponding diffraction patterns of 8 h traditional age formed component close to $[001]_{Al}$. Figure 11a, b shows the intragranular precipitate microstructure within the tensile stress layer. Many of the non-grown fine precipitates are about 15 nm in length. It can be deduced by diffraction line between the bright dots (Al matrix) that the precipitates are GP zones and θ″, as shown Fig. 11b. It is found that most of the precipitates are in a certain direction, which is so-called stress orientation effect [32]. It has been accepted that the preferential precipitation process of these coherent or semi-coherent second phase is affected by the elastic strain caused by the lattice misfits between the second-phase particles and the matrix. In addition, there are some coarse precipitates (marked with the red arrows) formed in the aluminum matrix. The high-resolution TEM picture attached in the Fig. 11a shows that the coarse precipitate is θ′. Figure 11c, d shows the morphology and species of precipitates in the compressive stress layer. Compared with the precipitate microstructure in tensile stress layer, the distribution of the precipitates is more homogeneous and the number density of precipitates is higher (Fig. 11c, d). Meanwhile, the number of θ′ phase is decreased (Fig. 11c). It indicated that the compressive stress can weaken the stress orientation effect and restrains the precipitation of θ′ phase during the age forming process. So far, it has been widely accepted that the stress orientation effect can weaken the performance of aluminum alloys. Furthermore, the coarse precipitates are also not conducive to strengthening basing on the Orowan mechanism. Therefore, the mechanical properties of the compressive layers are greater than that of

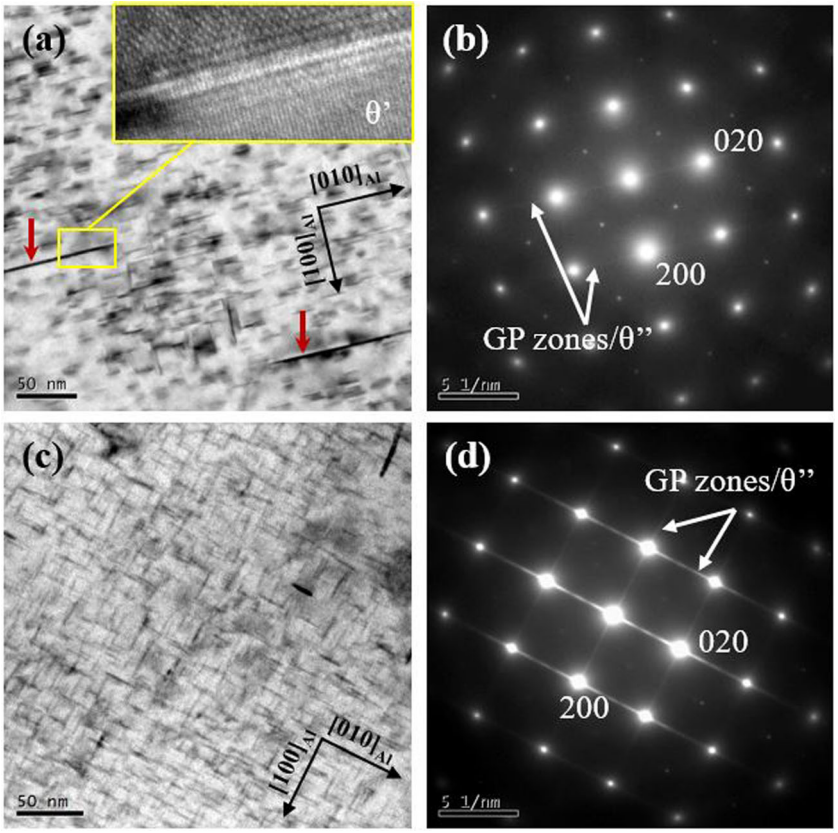

Fig. 11 TEM images and corresponding diffraction patterns of the traditional age formed component within **a**, **b** tensile stress layer and **c**, **d** compressive stress layer, respectively

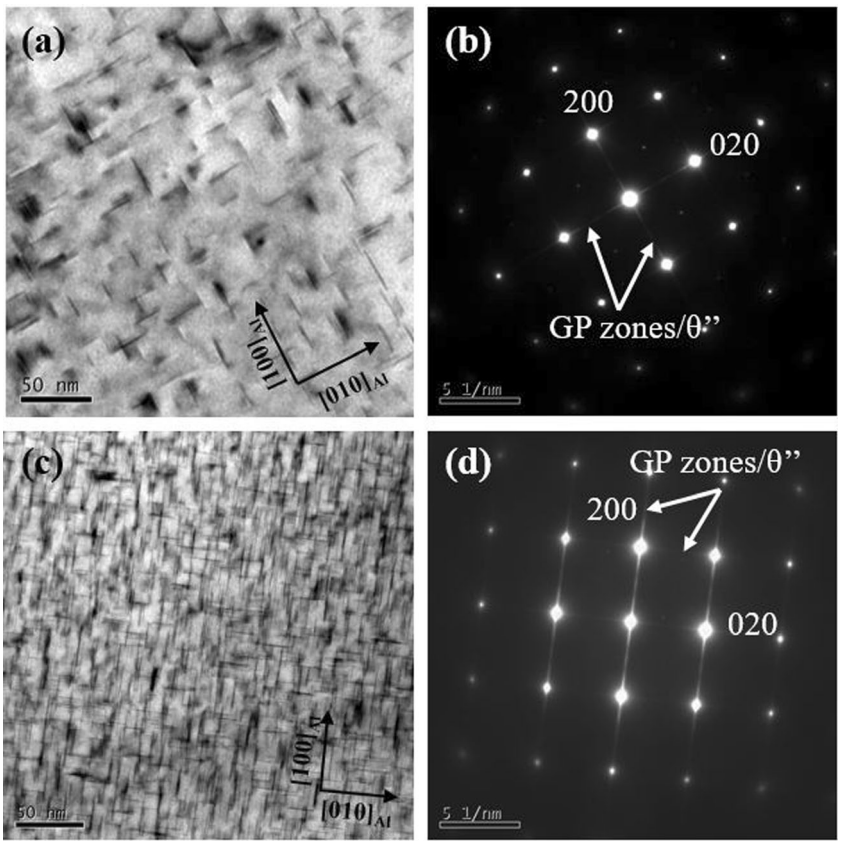

Fig. 12 TEM images and corresponding diffraction patterns of the pulse current assisted age formed component within **a**, **b** tensile stress layer and **c**, **d** compressive stress layer, respectively

Table 4 Statistical results of morphology and volume fraction of the matrix precipitates

Conditions	Diameter/ nm	Area fraction/ %	Volume fraction/ %
AFed-tension layer	14.56	13.42	1.60
AFed-compression layer	15.12	20.22	2.60
PCAAFed-tension layer	19.39	15.13	2.41
PCAAFed-compression layer	15.32	22.61	2.99

the tensile layers within the formed components (Table 3). Meanwhile, these coarser precipitates attract more solute atoms, which greatly reduce the number of precipitates in the matrix (Fig. 11a vs. 11c). Therefore, in the tensile stress layer, particles coarsening as an auxiliary agent besides lattice swelling had remarkable contribution in electrical conductivity enhancement through reducing the volume fraction of electron scattering agents (Fig. 10).

The TEM images and corresponding diffraction patterns of 8-h electric pulse assisted age formed component are shown in Fig. 11. For the precipitate microstructures in tensile layer (Fig. 12a, b), the size and number density of matrix precipitates of the PCAAFed component is larger than that of the AFed component, average precipitates' size is about 20 nm. At the same time, it is observed that the stress orientation effect is not obvious, indicating that the pulse current promotes the nucleation and growth of the matrix precipitates. As expected, the number density of precipitates in compressive stress layer is significantly greater than that in tensile stress layer of the PCAAFed component (Fig. 12a, c). However, more fine precipitates (GP zones and θ″ phase) and fewer θ′ phase formed in the PCAAFed component when compared with the precipitates in the AFed one. One possible explanation is that the pulse current promotes the homogenous nucleation of precipitates in the initial stage of the age forming process, and then inhibits the heterogeneous nucleation and coarsening of θ′ phase.

In order to compare the differences in the precipitates between the AFed and PCAAFed processes, the quantitative data of morphology and volume fraction of the matrix precipitates in two different processes conditions are reported in Table 4. The Length, width, and area fraction of the matrix precipitates can be obtained using TEM statistical investigations and image analysis (Image J).For each specimen, there are more than 300 measurements of matrix precipitates for determination of the average length and width. The volume fraction of disk-like precipitates can be calculated by the equation [33]:

$$f_v = \left(\frac{-2\pi d}{\pi d + 8h}\right)\ln\left(1-A_p\right)$$

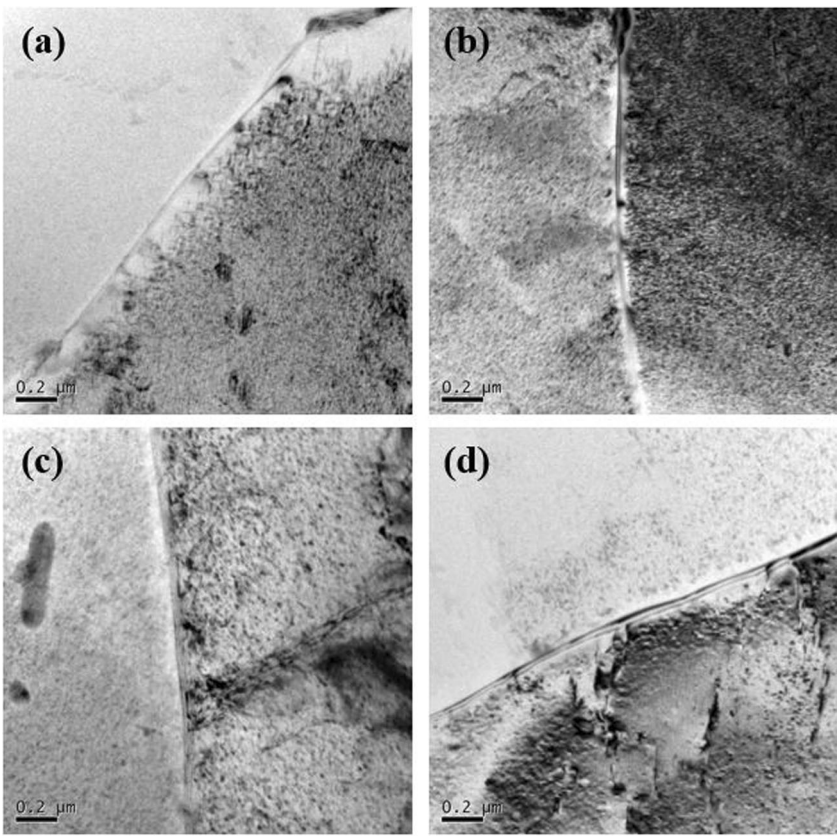

Fig. 13 TEM images of **a** tensile layer and **b** compressive layer of AFed and **c** tensile stress layer and **d** compressive stress layer of PCAAFed component

Here, d is the diameter of precipitates; h is the foil thickness (about 100 nm); and A_p represents for the area fraction of precipitates in the TEM images.

Two important results can be found in the Table 4. One of them is that the volume fractions of precipitates in the compression layer are higher than those in the tension layers. The other is that the PCAAFed component has greater volume fraction of precipitates when compared to the AFed component. It indicated that the pulse current promotes the nucleation and growth of precipitates during the age forming process. The main reason for this phenomenon is that the electromigration helps atomic diffusion. The more the fine precipitates are, the better the strengthening effect is. In a view of above (Fig. 11, Fig. 12, and Table 4), thus the mechanical properties of the EPAAFed component are superior to that of the AFed component (Table 3). Moreover, the aging process will consume a large amount of solute atoms. Therefore, the EPAAFed component has better electrical conductivity than the AFed one.

Figure 13 shows the difference in grain boundary microstructures between the EPAAFed and AFed components. It can be seen that precipitation free zone (PFZ) accompanying with the grain boundary formed in both two formed components. It is accepted that the broadened PFZ is detrimental to aluminum alloys' properties [34], especially stress corrosion resistance. For the AFed component, the width of the tensile stress layer is about 120 nm, and the compressive stress layer is about 101 nm. For the PCAAFed component, the grain boundary microstructure in the tensile stress layer and compressive layer have the same rule in width of PFZ. In addition, it can be seen form Fig. 13c, d that the widths of PFZ in PCAAFed component are more narrow than that in AFed component. The PFZ width of the tensile layer and the compressive layer in PCAAFed component is about 91 and 90 nm, respectively. This may be one of the reasons for the decrease in elongation of the formed component under compressive stress. However, one possible reason for the low electric conductivity of compressive stress layer in both AFed and PCAAFed component is that the compressive stress restrains the nucleation and growth of the θ′ phase (Figs. 11 and 12). After all, the coherent second phases of GP zones and θ″ also cause the lattice distortion in Al matrix. Meanwhile, it suggested that the EPAAF process could improve the stress corrosion resistance of the studied component.

4 Conclusion

The effects of pulse current on electric field, Joule heat effect, springback, mechanical properties, and precipitation microstructures of a 2219 aluminum alloy component were investigated. The main findings are as follows:

(1) The current density is centrally symmetric in the component under the pulse current assisted age forming condition. Comparing the simulation and tests, it is found that the influence of low-density pulse current (less than 80 A/cm^2) on the aging temperature can be ignored.
(2) The pulse current assisted age forming process can reduce the springback and the variation of the radius of different areas in formed components. It indicated that the pulse current assisted age forming process could improve the forming efficiency and precision of aluminum alloy components.
(3) The mechanical properties and electrical conductivity of the pulse current assisted age formed component are greater than that of the traditional age formed component. However, the effect of the pulse current on the mechanical properties anisotropy is not obvious. It indicated that the pulse current assisted age forming process could improve the comprehensive performance of the formed components.
(4) Compared with the traditional age forming process, the pulse current assisted age forming process can increase the number of the matrix precipitates, promote the distribution of precipitates. It showed that the pulse current assisted age forming process could promote the fine precipitates in aluminum matrix. Furthermore, it is possible to realize the shape and performance cooperative manufacturing of high-strength aluminum alloy components by optimizing the pulse current assisted age forming conditions.

Acknowledgements The authors would like to thank the National Key R&D Program of China (2017YFB0306300), the Key Program of National Natural Science Foundation of China (51235010, 51675538), the Project of Innovation-driven Plan in Central South University (2015CX002), the National Key Basic Research Development Plan Funded Project of China (2014CB046602), as well as the Fundamental Research Funds for the Central Universities of Central South University (1053320170641) for their financial support.

References

1. Pouraliakbar H, Firooz S, Jandaghi MR, Khalaj G, Nazari A (2016) Predicting the ultimate grain size of aluminum sheets undergone constrained groove pressing. Int J Adv Manuf Technol 86(5–8): 1639–1658. https://doi.org/10.1007/s00170-015-8212-x
2. Li J, Liu H (2015) Optimization of welding parameters for the reverse dual-rotation friction stir welding of a high-strength aluminum alloy 2219-T6. Int J Adv Manuf Technol 76(5–8):1469–1478. https://doi.org/10.1007/s00170-014-6352-z
3. Yang T, Xiong J, Chen H (2016) Effect of process parameters on tensile strength in plasma-MIG hybrid welding for 2219 aluminum alloy. Int J Adv Manuf Technol 84(9–12):2413–2421. https://doi.org/10.1007/s00170-015-7901-9

4. Pouraliakbar H, Pakbaz M, Firooz S, Jandaghi M, Khalaj G (2016) Study on the dynamic and static softening phenomena in Al–6Mg alloy during two-stage deformation through interrupted hot compression test. Measurement 77:50–53
5. Zhan L, Lin J, Dean T (2011) A review of the development of creep age forming: experimentation, modelling and applications. Int J Mach Tools Manuf 51(1):1–17
6. Lam AC, Shi Z, Lin J, Huang X, Zeng Y, Dean TA (2015) A method for designing lightweight and flexible creep-age forming tools using mechanical splines and sparse controlling points. Int J Adv Manuf Technol 80(1–4):361–372. https://doi.org/10.1007/s00170-015-6982-9
7. Luo H, Li W, Li C, Wan M (2017) Investigation of creep-age forming of aluminum lithium alloy stiffened panel with complex structures and variable curvature. Int J Adv Manuf Technol 91(9–12):3265–3271. https://doi.org/10.1007/s00170-017-0004-z
8. Xu Y, Zhan L, Li W (2017) Effect of pre-strain on creep aging behavior of 2524 aluminum alloy. J Alloy Compd 691:564–571
9. Yang Y, Zhan L, Ma Q, Feng J, Li X (2016) Effect of pre-deformation on creep age forming of AA2219 plate: Springback, microstructures and mechanical properties. J Mater Process Technol 229:697–702
10. Zhang J, Wang Y, Deng Y, Zhang X (2016) Effect of deformation degree on the creep age forming of 7475 aluminum alloy: the feasibility of the extended deformation range. Mater Sci Eng A 664:126–134
11. Li J, Li M, Liu D (2015) Influences of solution treatment in an electric field on creep age forming of 2A12 aluminum alloy sheets. Forg Stamp Tech 40(6):102–107
12. Xu Y, Zhan L, Ma Z, Huang M, Wang K, Sun Z (2017) Effect of heating rate on creep aging behavior of Al-cu-mg alloy. Mater Sci Eng A 688:488–497
13. Li Y, Shi Z, Lin J, Yang Y, Rong Q, Huang B, Chung T, Tsao C, Yang J, Balint D (2017) A unified constitutive model for asymmetric tension and compression creep-ageing behaviour of naturally aged Al-cu-li alloy. Int J Plasticity 89:130–149
14. Li Y, Shi Z, Lin J, Yang Y, Saillard P, Said R (2018) FE simulation of asymmetric creep-ageing behaviour of AA2050 and its application to creep age forming. Int J Mech Sci 140:228–240
15. Batalha G, Prados E, Ribeiro F, Scarpin B, Inforzato D, Costa P, Travessa D, (2014) 2.08 - Creep Age Forming Modeling and Characterization, Editor(s): Saleem Hashmi, Gilmar Ferreira Batalha, Chester J. Van Tyne, Bekir Yilbas, Comprehensive Materials Processing, Elsevier,149–159
16. Jeshvaghani R, Zohdi H, Shahverdi H, Bozorg M, Hadavi S (2012) Influence of multi-step heat treatments in creep age forming of 7075 aluminum alloy: optimization for springback, strength and exfoliation corrosion. Mater Charact 73:8–15
17. Huang G (2016) Effect of static electric field on the creep age forming of 7075 aluminum alloys. Hangkong University
18. Zhan L, Jia S, Zhang J (2014) Influence of electrical impulse aging on microstructure and mechanical properties of 7075 aluminum alloy. Trans Nonferrous Met Soc China 24(3):600–605
19. Zhan L, Ma Z, Zhang J, Tan J, Yang Z, Li H (2016) Stress relaxation ageing behaviour and constitutive modelling of a 2219 aluminium alloy under the effect of an electric pulse. J Alloy Compd 679:316–323
20. Yang Y, Zhan L, Shen R, Liu J, Li X, Huang M, Wan L (2018) Investigation on the creep-age forming of an integrally-stiffened AA2219 alloy plate: experiment and modeling. Int J Adv Manuf Technol 95(5):2015–2025. https://doi.org/10.1007/s00170-017-1248-3
21. Xu Y, Zhan L, Huang M, Shen R, Ma Z, Xu L, Wang X (2018) Deformation behavior of Al-cu-mg alloy during non-isothermal creep age forming process. J Mater Process Technol 255:26–34
22. Liu Y, Huang M, Ma Z, Zhan L (2016) Influence of the low-density pulse current on the ageing behavior of AA2219 aluminum alloy. J Alloy Compd 673:358–363
23. Tan J, Zhan L, Zhang J, Yang Z, Ma Z (2016) Effects of stress relaxation aging with electrical pulses on microstructures and properties of 2219 aluminum alloy. Materials 9(7):538
24. Zhang J, Zhan L, Jia S (2014) Eeffects of electric pulse current on the aging kinetics of 2219 aluminum alloy. Adv Mater Sci Eng 2014(8):1–8
25. Brandão F, Delijaicov S, Bortolussi R (2017) CAF-a simplified approach to calculate springback in Al 7050 alloys. Int J Adv Manuf Technol 91(9–12):3273–3284. https://doi.org/10.1007/s00170-016-9839-y
26. Xu Y, Zhan L (2016) Effect of creep aging process on microstructures and properties of the retrogressed Al-Zn-mg-cu alloy. Metals 6(8):189
27. Xu Y, Zhan L, Huang M, Shen R (2017) Numerical simulation of temperature field in large integral panel during age forming process: effect of autoclave characteristics. Process Eng 207:269–274
28. Lei C, Yang H, Li H, Shi N, Fu J, Zhan L (2016) Dependence of creep age formability on initial temper of an Al-Zn-mg-cu alloy. Chinese J Aeronaut 29(5):1445–1454
29. Pouraliakbar H, Jandaghi M, Khalaj G (2017) Constrained groove pressing and subsequent annealing of Al-Mn-Si alloy: microstructure evolutions, crystallographic transformations, mechanical properties, electrical conductivity and corrosion resistance. Mater Des 124:34–46
30. Jandaghi M, Pouraliakbar H, Shiran M, Khalaj G, Shirazi M (2016) On the effect of non-isothermal annealing and multi-directional forging on the microstructural evolutions and correlated mechanical and electrical characteristics of hot-deformed Al-mg alloy. Mater Sci Eng A 657:431–440
31. Popov B (2015) Chapter 9-stress corrosion cracking. In: Corrosion engineering. Elsevier, Amsterdam, pp 365–450
32. Yang Y, Zhan L, Shen R, Yin X, Li X, Li W, He D (2017) Effect of pre-deformation on creep age forming of 2219 aluminum alloy: experimental and constitutive modelling. Mater Sci Eng A 683:227–235
33. Krug M, Mao Z, Seidman D, Dunand D (2014) Comparison between dislocation dynamics model predictions and experiments in precipitation-strengthened Al–li–Sc alloys. Acta Mater 79:382–395
34. Xu Y, Zhan L, Xu L, Huang M (2017) Experimental research on creep aging behavior of Al-cu-mg alloy with tensile and compressive stresses. Mater Sci Eng A 682:54–62